JOURNAL OF VIROLOGY, Aug. 2001, p. 7494–7505 Vol. 75, No. 16
0022-538X/01/$04.00+0 DOI: 10.1128/JVI.75.16.7494–7505.2001

Prolonged Gray Matter Disease without Demyelination Caused by Theiler's Murine Encephalomyelitis Virus with a Mutation in VP2 Puff B

IKUO TSUNODA,[1] YOSHIAKI WADA,[1]† JANE E. LIBBEY,[1] THOMAS S. CANNON,[1] FRANK G. WHITBY,[2] AND ROBERT S. FUJINAMI[1]*

Department of Neurology, University of Utah School of Medicine,[1] and Department of Biochemistry, University of Utah,[2] Salt Lake City, Utah 84132

Received 5 February 2001/Accepted 2 May 2001

Theiler's murine encephalomyelitis virus (TMEV) is divided into two subgroups based on neurovirulence. During the acute phase, DA virus infects cells in the gray matter of the central nervous system (CNS). Throughout the chronic phase, DA virus infects glial cells in the white matter, causing demyelinating disease. Although GDVII virus also infects neurons in the gray matter, infected mice developed a severe polioencephalomyelitis, and no virus is detected in the white matter or other areas in the CNS in rare survivors. Several sequence differences between the two viruses are located in VP2 puff B and VP1 loop II, which are located near each other, close to the proposed receptor binding site. We constructed a DA virus mutant, DApBL2M, which has the VP1 loop II of GDVII virus and a mutation at position 171 in VP2 puff B. While DApBL2M virus replicated less efficiently than DA virus during the acute phase, DApBL2M-induced acute polioencephalitis was comparable to that in DA virus infection. Interestingly, during the chronic phase, DApBL2M caused prolonged gray matter disease in the brain without white matter involvement in the spinal cord. This is opposite what is observed during wild-type DA virus infection. Our study is the first to demonstrate that conformational differences via interaction of VP2 puff B and VP1 loop II between GDVII and DA viruses can play an important role in making the transition of infection from the gray matter in the brain to the spinal cord white matter during TMEV infection.

Theiler's murine encephalomyelitis virus (TMEV) belongs to the family *Picornaviridae* and is divided into two subgroups based on neurovirulence in mice, i.e., GDVII and TO (14, 41, 42). Strains in the first subgroup, GDVII, include the highly neurovirulent GDVII and FA strains, infect neurons in the gray matter of the central nervous system (CNS), and cause an acute polioencephalomyelitis with extensive apoptosis of neurons. Most mice infected with GDVII virus die within 10 days (43), and the virus has never been isolated from the rare survivor (22). The second subgroup, TO, including DA and BeAn strains, causes a biphasic disease. Similar to GDVII virus, DA virus infects neurons in the gray matter, mainly in the brain, and causes polioencephalomyelitis with mild neuronal apoptosis 1 week after infection (the acute phase). However, the mice survive the acute phase and progress to develop a chronic demyelinating disease in the white matter of the spinal cord 1 month postinfection (the chronic phase). During the chronic phase, virus or viral products are detected in glial cells and macrophages in the white matter of the spinal cord but not in the neurons of the brain. This chronic phase is a well-characterized experimental animal model for multiple sclerosis (2, 4, 31, 41, 42).

We do not know why GDVII virus predominantly infects neurons in the gray matter is not known, and the mechanism by which DA virus infects neurons in the gray matter during the acute phase and persistently infects glial cells and macrophages in the white matter during the chronic phase has not been identified. This hampers the clarification of the pathogenesis of TMEV infection and mechanism(s) of viral persistence and demyelination. One hypothesis is that the difference(s) in the receptor binding site between GDVII and DA viruses contributes to the difference in host cell tropism (49).

Although the receptor for TMEV in the host cell is unknown, the pit, or depression surrounding the fivefold axis of picornavirus, is believed to be the receptor binding site (10, 23, 29, 34). In contrast to the other picornaviruses, TMEV has unique loop structures, which are made up of connections of the β strands, near the fivefold vertices at the edge of the pit. There are four large loops that extend nearly perpendicular to the surface of the virion: two are between the CD strands of VP1 (loop I and II), and two are between the EF strands of VP2 (puff A and puff B) (26, 49). Zhou et al. reported that VP2 puff B also influenced the shape of a gap between VP1 and VP2 on the capsid surface next to the putative receptor binding site (51). They speculated that the gap might be important in determining viral persistence by influencing virus attachment to cellular receptors (51). Exposed amino acids on all the loops have been shown to be important disease determinants. Amino acid changes in positions 81 (loop I) (26) and 101 (loop II) (17, 21, 50, 52) of VP1 and in positions 141 of puff A (15, 36) and 173 of puff B (17, 36) of VP2 have resulted in viruses with altered disease phenotypes (14).

Despite the overall structural similarity between GDVII virus and the two less virulent DA and BeAn viruses, three sites

* Corresponding author. Mailing address: Department of Neurology, University of Utah School of Medicine, 30 North 1900 East, Room 3R330, Salt Lake City, UT 84132. Phone: (801) 585-3305. Fax: (801) 585-3311. E-mail: Robert.Fujinami@hsc.utah.edu.

† Present address: Department of Neurology, Nissan Tamagawa Hospital, 4-8-1 Seta, Setagaya-ku, Tokyo 158-0095, Japan.

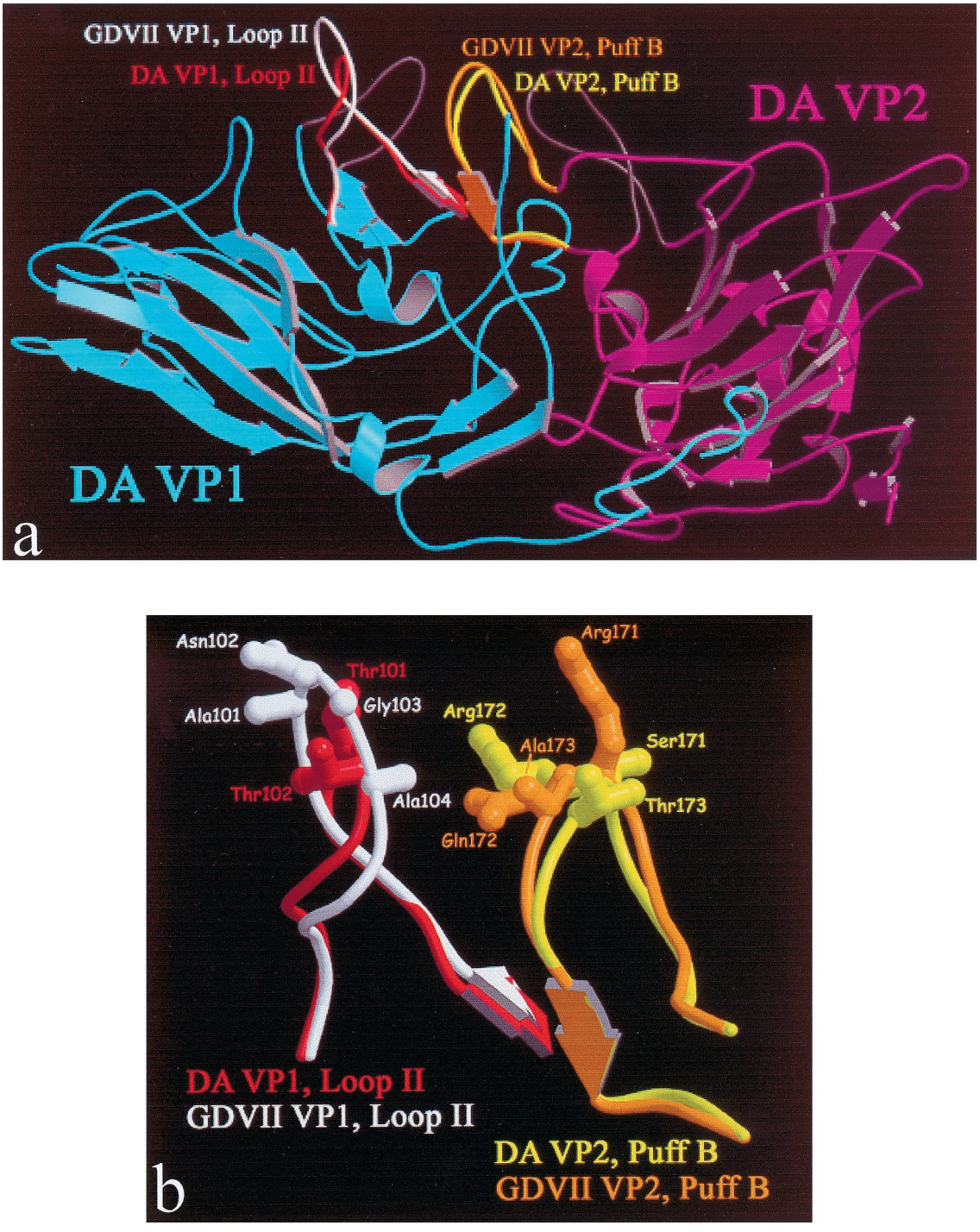

FIG. 1. (a) Ribbon representation of TMEV constructs. Shown in blue and purple are DA strain VP1 and VP2, respectively. DA strain VP1 loop I and VP2 puff A are colored dark gray at top center in the rear plane (not labeled). DA strain VP1 loop II and VP2 puff B are shown in red and yellow, respectively. GDVII strain VP1 loop II and VP2 puff B are shown in white and orange, respectively. (b) Model of the expected differences in TMEV constructs. Loop regions are shown for the superimposition of DA and GDVII strains. Panel a is a large view, while panel b is a detail view.

of the GDVII virus structure show local differences: residues 170 to 173 of VP2 on puff B, the knob of VP3, and the loop II of VP1 (24). These differences mainly involve side chains. Puff B of VP2 and loop II of VP1 are near each other (Fig. 1a). Amino acid differences between GDVII and DA viruses are shown in Fig. 1b and Table 1 (27, 36). There is a deletion of two amino acids (GA) and two substitutions (A-T and N-T) in the DA loop II. In residues 170 to 173 of VP2 on puff B, there are three amino acid substitutions (at positions 171 to 173) between the two viruses.

TABLE 1. VP1 loop II and VP2 puff B

Virus[a]	Sequence[b]	
	VP1 loop II (94–111)	VP2 puff B (164–181)
GDVII	RWVRSGGANGANFPLMTK	PTGYRYDRQAGFFAMNHQ
DA	RWVRSGGTT - - NFPLMTK	PTGYRYDSRTGFFAMNHQ
DApB	RWVRSGGTT - - NFPLMTK	PTGYRYD**RQV**GFFAMNHQ
DApBL2M	RWVRSGG**ANGA**NFPLMTK	PTGYRYD**R**RTGFFAMNHQ
DA8	RWVRSGG**ANGA**NFPLMTK	PTGYRYDSRTGFFAMNHQ

[a] DA virus lacks two amino acids between positions 102 and 103 of VP1 loop II. At amino acid position 178 of VP2 puff B, the DA virus used in our laboratory has a M instead of N (reference 22 and unpublished data). DApB virus was constructed to mimic VP2 puff B of GDVII virus in the background of DA virus. The amino acid substitutions in the mutants are shown in boldface. DApBL2M virus has VP1 loop II of GDVII with a mutation in VP2 puff B in the background of DA virus. DA8 virus has VP1 loop II of GDVII virus in the background of DA virus (49).

[b] Differences in amino acid sequences of the neurovirulent GDVII virus and the persistent pDA virus are underlined (24).

Previously we investigated the role of VP1 loop II of TMEV during both the acute and the chronic phases of TMEV infection (49, 50, 53). If the amino acid at position 101 (threonine) of VP1 loop II of DA virus was replaced by an isoleucine or alanine or two amino acids (GA) were inserted after the threonine, the ability of the mutant viruses to persist was either markedly reduced or lost. From these data, we hypothesized that the changes in loop II between GDVII and DA viruses could contribute to biological differences in phenotype between the viruses. We next generated the DA mutant virus DA8, which has the entire loop II of GDVII virus in the background of DA virus (Table 1) (49). DA8 virus induced an acute polioencephalomyelitis and a demyelinating disease comparable to that induced by wild-type DA virus. These findings suggest that the structural integrity, not the specific sequence in this region, was a requirement for DA virus tropism and persistence. In addition, the difference in VP1 loop II alone could not account for the lack of virus infection of the spinal cord white matter or absence of demyelination in GDVII virus infection.

In this study, we focused on the VP2 puff B and its interaction with VP1 loop II, relating to tropism and pathogenesis. VP2 puff B forms a short two-stranded antiparallel β sheet with loop II in VP1 via interactions of residues 94 to 96 in VP1 and residues 176 to 178 in VP2 (23). Any mutation on loop II of VP1 is likely to alter the interaction, which may result in conformational changes of the VP2 puff B. This would suggest that interactions between subunits via loops might have a direct effect on virus-host interactions and viral pathogenesis (15, 16, 23). We hypothesized that the conformational difference(s) in VP2 puff B and/or different interactions of VP2 puff B and VP1 loop II between GDVII and DA viruses play a role in creating a critical structure for virus-cell interaction, contributing to the different host range and disease phenotype.

Using site-directed mutagenesis, we constructed recombinant TMEVs. One mutant virus, DApB, mimics the VP2 puff B of GDVII virus in the background of DA virus; the other mutant virus, DApBL2M, has the VP1 loop II of GDVII virus with an additional mutation (S-R substitution at position 171) in VP2 puff B in the background of DA virus. All viruses replicated to similar titers in vitro. Although both mutants replicated less efficiently in the CNS than wild-type DA (pDA virus), they induced an acute poliencephalitis comparable to DA infection. During the chronic phase, mice infected with DApB virus developed an attenuated demyelinating disease in the white matter of the spinal cord. In contrast, mice infected with DApBL2M virus did not have white matter lesions in the spinal cord but had gray matter lesions in the brain. Therefore, the replacement of VP1 loop II of the DA virus with that of GDVII virus plus an additional mutation in VP2 puff B most likely allowed the mutant TMEV, DApBL2M, to continue to infect gray matter neurons in the brain during the chronic phase. We think that these changes did not allow infection of white matter glial cells in the spinal cord, thus inhibiting the demyelinating disease. Although several TMEV mutants with changes in loop structures have been studied, this is the first study to demonstrate that conformational differences via interaction of VP2 puff B and VP1 loop II between GDVII and DA viruses can play an important role in making the transition of infection from the gray matter in the brain to the spinal cord white matter in TMEV infection.

MATERIALS AND METHODS

Construction of DA virus mutants. Mutant DApB was generated by in vitro site-directed mutagenesis using PCR with pDAFL3 as a template. pDAFL3 is a transcription vector that contains the entire cDNA of the DA strain and was kindly provided by Raymond P. Roos, University of Chicago (33). Two oligonucleotides containing the mutation were designed for DApB to change four bases between nucleotide positions 2019 and 2023 (2019, 2021, 2022, and 2023): 2019+ (5′CGATAG**ACAAG**CCGGTTTCTTCGCCATG3′) and 2019− (5′AAGAAAC CGG**CTTGT**CTATCGTAGCGGTAA3′). The nucleotide substitutions are in boldface. Two additional oligonucleotides were designed to allow extension from the mutation site to positions 1825 and 2941: 1825 (5′AAGACCGGCTGGCG AGTACAAGTTCA3′) and 2197 (5′TGAAGACGGCAACGACGAGGGTCC AATTA3′). We performed two PCR amplification (1825 to 2033 and 2013 to 2941) using GeneAmp kit reagents and a thermocycler (Perkin-Elmer Cetus, Norwalk, Conn.). The PCR products were mixed, and a second PCR, overlapping extension PCR, was conducted.

The PCR product was digested with *Sph*I and *Nco*I. pDAFL3 was digested with *Sph*I and *Xho*I and with *Nco*I and *Xho*I (Gibco, Gaithersburg, Md.). The 0.2-kb PCR product and 10- and 0.7-kb fragments from pDAFL3 were isolated and ligated with T4 DNA ligase (Gibco). Transformation into *Escherichia coli* DH5α competent cells was performed according to the vendor's protocol. Plasmid DNAs were extracted by the alkali-sodium dodecyl sulfate method. These DNAs were digested with *Age*I-*Bgl*II and *Nco*I to confirm the mutation and the proper orientation of the fragments. For clones selected by enzyme digestion, the insertion fragment synthesized by PCR was sequenced using a T7 sequencing kit (Pharmacia, Piscataway, N.J.) to confirm the mutation. The infectious cDNA clone was named pDApB.

The other mutant, DApBL2M, was generated from pDApB and pDA8, which contains the entire VP1 loop II of GDVII virus (49). pDApB and pDA8 were digested with *Kpn*I and *Pfl*MI. The 2-kb fragment from pDApB and 9-kb fragment from pDA8 were isolated and ligated. After transformation into DH5α cells, plasmid DNAs were extracted and digested with *Kpn*I and *Nco*I to confirm the mutation. The infectious cDNA clone was named pDApBL2M.

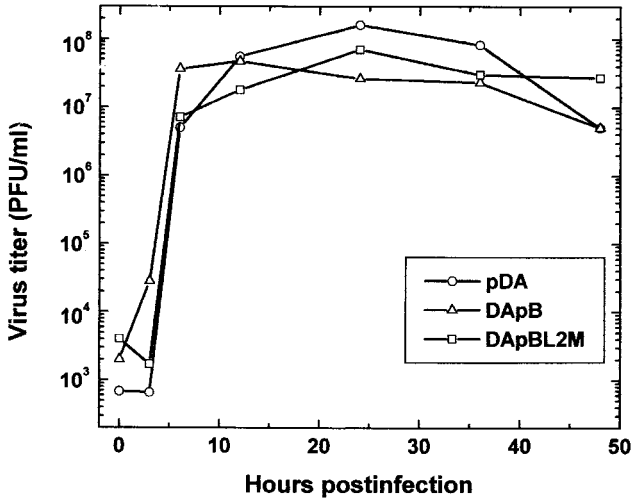

FIG. 2. One-step growth curve of TMEV mutants. We infected BHK-21 cells with wild-type pDA, DApB and DApBL2M viruses at an MOI of 5. Infected cells with supernatants were harvested at the indicated time points, and the virus titers were determined by a plaque assay. We could detect comparable amounts of viruses between the groups. Results are representative of two independent experiments.

Cell, transfection, and virus. BHK-21 cells (American Type Culture Collection, Manassas, Va.) were maintained in Dulbecco's modified Eagle medium (Gibco). In vitro transcription reactions of pDAFL3, pDApB, and pDApBL2M were performed as previously described (50). RNA obtained from an in vitro transcription reaction was transfected into BHK-21 cells by lipofection (Gibco). Viruses plaque purified from the original transfection stock made in BHK-21 cells were used to generate working pools. Viruses obtained from pDAFL3, pDApB, and pDApBL2M transfections were named pDA, DApB, and DApBL2M. After plaque purification, DApBL2M was found to have a point mutation at position 171 in puff B. Other plaques from that original pool had the same point mutation.

Viral RNA was isolated from viral pools by using TRIzol Reagent (Gibco) according to the manufacturer's instructions. The RNA was subjected to reverse transcription (RT) PCR (RT-PCR) using a Ready-To-Go You-Prime First-Strand Beads kit (Pharmacia) according to the manufacturer's instructions. The primers used for RT, PCR, and subsequent sequencing of the PCR product were DA virus VP1 loop II and VP2 puff B specific. The PCR product of the appropriate size was band isolated from a gel via a QIAquick gel extraction kit (Qiagen, Chatsworth, Calif.) according to the manufacturer's instructions prior to sequencing by the University of Utah Sequencing Facility.

One-step growth curve. BHK-21 cells in six-well plates were infected with a multiplicity of infection (MOI) of 5 PFU per cell with each virus and allowed to adsorb for 1 h at 37°C. After 1 h of adsorption, the wells were washed with phosphate-buffered saline (PBS) three times and 3 ml of complete Dulbecco's modified Eagle medium supplemented with 2% fetal bovine serum was added. At various times after adsorption, the infected cells with supernatants were collected. Samples were frozen and thawed three times, and viral titers were determined by a plaque assay (26). The limit of detection for the plaque assay was 5 PFU of virus per ml. Virus titration was performed in duplicate. Results are representative of two independent experiments.

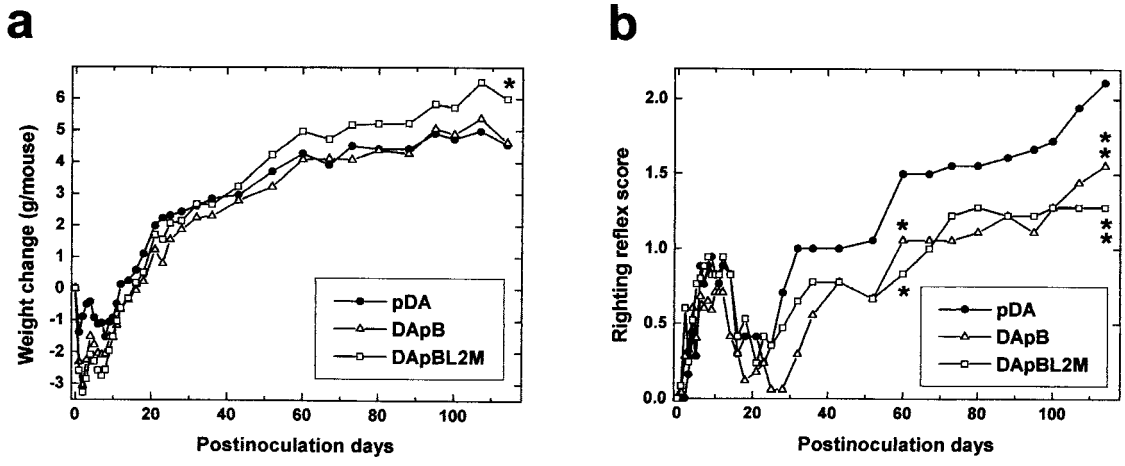

FIG. 3. Clinical signs in TMEV infection. We injected SJL/J mice with pDA, DApB, or DApBL2M virus intracerebrally and observed weight change (a) and righting reflex (b). In the first 2 weeks after infection, the acute phase, all groups showed weight loss and a mild impaired righting reflex. During the chronic phase, more than 1 month after infection, pDA and DApB virus infected mice showed less weight gain than DApBL2M virus-infected mice (weight gains on day 114: pDA, 4.5 ± 0.3 g; DApB, 4.6 ± 0.3 g; DApBL2M, 6.0 ± 0.5; $*P < 0.05$ compared with pDA, analysis of variance). The righting reflex abnormality was less severe in DApB and DApBL2M virus-infected mice than in pDA virus-infected mice (righting reflex scores on day 114: pDA, 2.1 ± 0.1; DApB, 1.6 ± 0.1; DApBL2M, 1.3 ± 0.2; **, $P < 0.01$). Each experimental group consisted of 5 to 16 mice. Results are representative of two independent experiments.

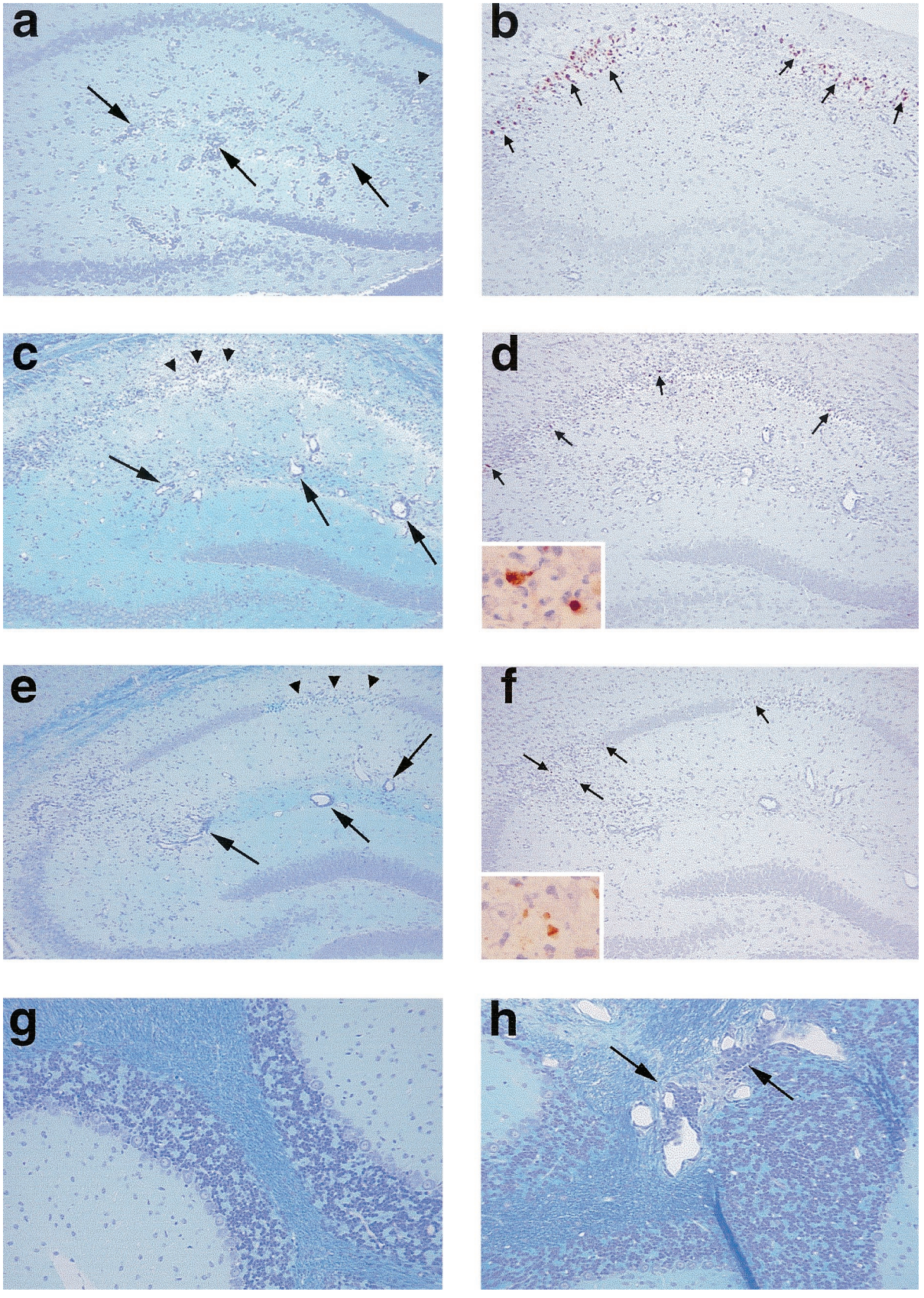

FIG. 4. Neuropathology during the acute phase of TMEV infection. Mice were sacrificed 1 week after infection with pDA (a, b, and g), DApB (c and d), or DApBL2M (e, f, and h) virus. In all groups, mice developed similar inflammatory responses in the hippocampal fissure (a, c, and e,

TABLE 2. Acute- and chronic-phase neuropathology in pDA, DApB, or DApBL2M virus infection[a]

Infection	Cerebral cortex	Olfactory nucleus	Hippocampus	Thalamus	Hypothalamus	Cerebellum	Pons	Spinal cord	
								Gray matter	White matter
Acute phase									
pDA	+++	+	++++	++	++	−	+	++	−
DApB	+++	+	++++	++	+	−	++	++	−
DApBL2M	+++	+	++++	++	+	+	++	++	−
Chronic phase									
pDA	−	−	−	−	−	−	+[b]	−	++++
DApB	−	−	±	±	−	±	+[b]	−	++
DApBL2M	±	−	+[b]	−	−	+[b]	+	−	−

[a] Five mice were injected intracerebrally with pDA, DApB, or DApBL2M virus and sacrificed during the acute phase, 1 week postinfection, and during the chronic phase, 1 and 4 months postinfection. The severity of each involved area was scored − to ++++ depending on the average number of lesions: −, no lesion; ±, fewer than 5 lesions detected in some mice; +, fewer than 5 lesions in all mice; ++, 5 to 20 lesions; +++, over 20 lesions; ++++, over 30 lesions. Since lesion distributions were similar at 1 and 4 months postinfection, we pooled scores during the chronic phase. Scores are means of 10 and 20 mice examined during the acute and chronic phases, respectively. Results are a combination of two independent experiments.

[b] During the chronic phase, although we found mild lesions in the white matter of the brainstem in pDA and DApB virus-infected mice, we could detect lesions in the gray matter of the hippocampus and cerebellum in DApBL2M virus-infected mice.

Animal experiments. Four-week-old female SJL/J mice were purchased from the Jackson Laboratory (Bar Harbor, Maine). Anesthetized mice were infected with 2×10^5 PFU of wild-type (pDA virus) or mutant TMEV in the right cerebral hemisphere. Mice were weighed and observed for clinical signs daily during the acute phase of disease and biweekly for 4 months during the chronic phase. Clinical signs of TMEV infection were evaluated by an impaired righting reflex (30, 40). When the proximal end of the mouse's tail is grasped and twisted first to the right and then to the left, a healthy mouse resists being turned over (score of 0). If the mouse is flipped onto its back but immediately rights itself on one side or both sides, it is given a score of 1 or 1.5, respectively. If it rights itself in 1 to 5 s, the score is 2. If righting takes more than 5 s, the score is 3.

Histology. Mice were euthanized with halothane after the 4-month observation period. We perfused mice with PBS followed by phosphate-buffered 4% paraformaldehyde. Sections of brains (divided into 5 coronal slabs) and spinal cords (divided into 10 horizontal slabs) were embedded in paraffin. Four-micrometer-thick sections were stained with luxol fast blue for myelin visualization. Histological scoring was performed as previously described (44–47). Brain sections were scored for meningitis (0, no meningitis; 1, mild cellular infiltrates; 2, moderate cellular infiltrates; 3, severe cellular infiltrates) and perivascular cuffing (0, no cuffing; 1, 1 to 10 lesions; 2, 11 to 20 lesions; 3, 21 to 30 lesions; 4, 31 to 40 lesions; 5, over 50 lesions). Each score from the brain was combined for a maximum mononuclear cell (MNC) infiltration score of 8 per mouse. For scoring of spinal cord sections, each spinal cord section was divided into four quadrants: the ventral column, the dorsal column, and each lateral column. Any quadrant containing meningitis, demyelination, or perivascular cuffing was given a score of 1 in that pathologic class. The total number of positive quadrants for each pathologic class was determined, then divided by the total number of quadrants present on the slide, and multiplied by 100 to give the percent involvement for each pathologic class. TMEV antigen-positive cells were detected by the avidin-biotin peroxidase complex technique, using hyperimmune rabbit serum to DA virus (44–47). Enumeration of TMEV antigen-positive cells was carried out with a light microscope at a magnification of ×200, using 5 coronal brain sections and 10 horizontal sections per mouse as described previously (47). TMEV genome was detected by in situ hybridization using a digoxigenin RNA labeling kit (S6/T7; Roche Molecular Biochemicals, Mannheim, Germany) and alkaline phosphatase-conjugated antidigoxigenin antibody (Roche). 5-Bromo-4-chloro-3-indolylphosphate (BCIP) was used with nitroblue tetrazolium (NBT) as the substrate.

CNS viral titers. Infected mice were euthanized and perfused with PBS at 1 week, 1 month, and 4 months postinfection. The brains and spinal cords were aseptically removed, weighed, and homogenized in PBS. The homogenates were frozen and thawed three times and plaqued on BHK-21 cell monolayers (26, 46).

ELISA. Mice were bled from the tail vein upon arrival and at the time of sacrifice. Using an enzyme-linked immunosorbent assay (ELISA), we measured concentrations of serum anti-TMEV antibodies as described previously (26, 47). DA virus antigen was prepared by infecting BHK-21 cells with DA virus at an MOI of 0.1 PFU/cell as described by Kurtz et al. (18). Ninety-six well plates were coated overnight with DA virus antigen at 4°C. After blocking with diluent (PBS, 10% fetal bovine serum, 0.2% Tween 20), twofold dilutions of the mouse sera beginning at $1:2^7$ were added to the plates and incubated at room temperature for 90 min. After being washed with PBS containing 0.2% Tween 20, the plates were incubated with a goat anti-mouse peroxidase-labeled antibody in diluent for 90 min. The plates were colorized with *o*-phenylenediamine dihydrochloride (Sigma Chemical Co., St. Louis, Mo.) and were read at 492 nm on a Titertek Multiskan Plus MK II spectrophotometer (Flow Laboratories, McLean, Va.). The endpoint of the assay was determined as the reciprocal of the highest dilution that gave an optical density reading that was 2 standard deviations above the control baseline from preimmune sera.

RESULTS

Generation of mutant viruses. We constructed mutant infectious cDNA clones pDApB and pDApBL2M, which had a mutation in VP2 puff B alone or accompanied by VP1 loop II of GDVII virus in the background of DA virus. Viruses were plaque purified from virus pools. Consequently, one mutant, DApB, generated from pDApB, mimics the VP2 puff B of GDVII with one conservative change from pDApB (A to V) (Table 1). The other mutant, DApBL2M, generated from pDApBL2, has a point mutation at position 171 in VP2 puff B and the VP1 loop II of GDVII virus in the background of DA virus (Table 1).

In vitro virus replication. To assess whether the mutant viruses were replication competent, BHK-21 cells were infected with pDA, DApB, or DApBL2M virus, and one-step growth curves among the viruses were compared. As seen in

large arrow). More pyknotic neurons in the pyramidal cell layer (a, c, and e, arrowheads) of the hippocampus in DApB (c) and DApBL2M (e) virus-infected mice were observed. We detected more TMEV antigen-positive cells (b, d, and f, small arrows) in pDA virus-infected mice (b) than in DApB (d, inset) or DApBL2M (f, inset) virus-infected mice. Although the cerebellum was normal in pDA (g) or DApB virus-infected mice, DApBL2M virus-infected mice showed MNC inflammation (h, large arrows) in the cerebellum. (a, c, e, g, and h) Luxol fast blue stain; b, d, and f, immunohistochemistry for TMEV antigen. Magnifications: a to f, ×75; g and h, ×150; inset, ×320.

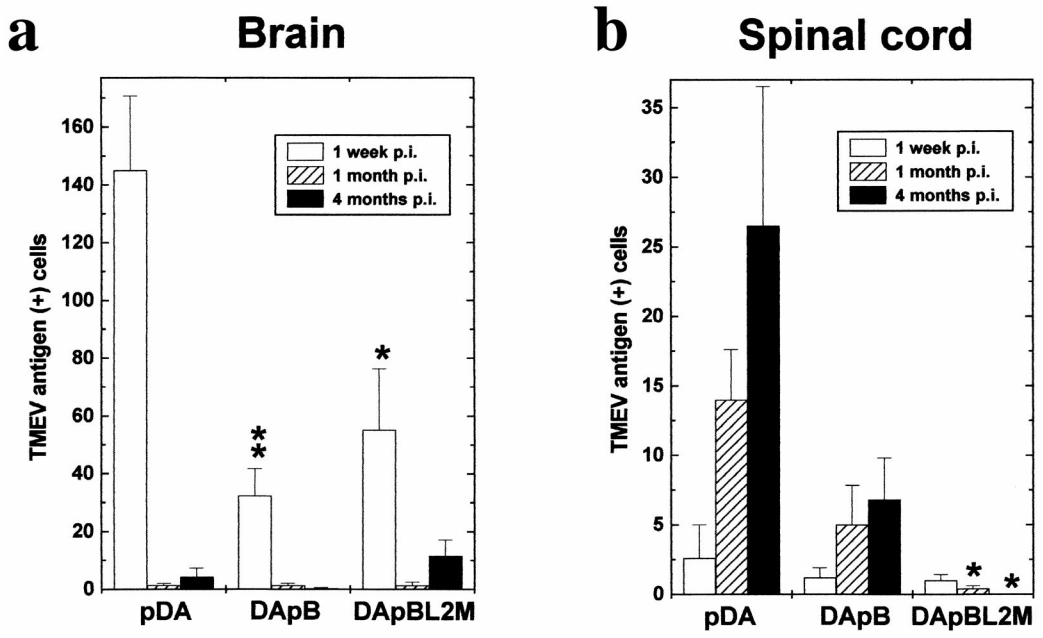

FIG. 5. Detection of TMEV antigen-positive cells in the CNS by immunohistochemistry. In the brain (a), we detected more viral antigens in all groups during the acute phase, 1 week postinfection (p.i.) pDA virus-infected mice contained significantly more antigen-positive cells than DApB (**, $P < 0.01$) or DApBL2M (*, $P < 0.05$) virus-infected mice. During the chronic phase, while a few viral antigen-positive cells were detected in the white matter in the brainstem after pDA and DApB virus infection, viral antigen was detected in the gray matter, particularly in the pyramidal cell layer of the hippocampus after DApBL2M virus infection. In the spinal cord (b), more viral antigen-positive cells were detected during the chronic phase, 1 and 4 months after infection, in the mice infected with pDA or DApB virus. Few viral antigen-positive cells were seen in DApBL2M virus-infected mice (*, $P < 0.05$ compared with pDA, analysis of variance). Values are mean antigen-positive cells per mouse ± standard error of the mean for five to six mice.

Fig. 2, we could detect comparable amounts of viruses in all groups.

GDVII and DA viruses have different plaque morphologies (22). GDVII virus produces large plaques on BHK cells (3.20 ± 0.19 mm) (26), while DA virus creates small plaques (0.96 ± 0.09 mm). Both DApB and DApBL2M viruses, like pDA virus, produced small plaques (DApB, 0.78 ± 0.1 mm; DApBL2M, 0.93 ± 0.14 mm).

Clinical disease. SJL/J mice were infected intracerebrally with pDA, DApB, or DApBL2M virus and observed for clinical signs for up to 4 months (Fig. 3). During the acute phase, within 2 weeks after infection, all groups of mice showed weight loss and an impaired righting reflex. No significant clinical differences were seen among the groups during the acute phase. By 3 weeks postinfection, most mice recovered from this acute disease without residual sequelae.

During the chronic phase, pDA virus-infected mice are known to show an impaired righting reflex 1 month after infection. As the disease progresses, the mice gain less weight (46) and obvious clinical signs (waddling gait and spastic paralysis of hind limb) are evident from 2 months postinfection (40, 47). Similarly, DApB virus-infected mice also gained less weight over this time. The other clinical signs, including an impaired righting reflex, were detected later and were milder than those of pDA virus-infected mice. In contrast, DApBL2M virus-infected mice showed only a mildly impaired righting reflex without gait abnormalities during the chronic phase. Once present, the clinical disease did not progress after day 70 (Fig. 3). In addition, DApBL2M virus-infected mice gained more weight than pDA virus-infected mice ($P < 0.05$).

Acute-phase neuropathology. During the acute phase, 1 week after infection, all the groups of mice developed polioencephalomyelitis, and lesions were mainly found in the gray matter of the brain (Table 2). In pDA virus-infected mice, we could see MNC infiltrates in perivascular spaces and in the meninges. The hippocampus, cerebral cortex, thalamus, substantia nigra (28, 39), and anterior horn of the spinal cord were also frequently affected (Fig. 4; Table 2). Meningitis was mild in both the brain and the spinal cord. The other lesions seemed to be associated with the limbic system, including the olfactory nuclei, the septal area, and the mamillary nuclei (39, 48). In DApB and DApBL2M virus-infected mice, the overall distribution and severity of the inflammatory lesions were similar to those seen in pDA virus-infected mice (Table 2; Fig. 4). We also compared the mean total MNC infiltration scores in the brain between viruses and found no differences (pDA, 6.6 ± 0.2; DApB, 6.0; DApBL2M, 6.0 [standard deviation for the latter two was 0]). Interestingly, however, frequent MNC inflammation was present in the cerebella of DApBL2M virus-infected mice (Fig. 4h). Involvement of the cerebellum is rare in wild-type TMEV infection (38). We found cerebellum involvement in neither pDA (Fig. 4g) nor DApB virus-infected mice. The pontine tegmentum tended to be more involved in the mice infected with either mutant (Table 2). In addition, we found more extensive apoptosis of neurons in the thalamus, hippocampus, and pons of mice infected with DApB or

DApBL2M virus than in those of mice infected with pDA virus (I. Tsunoda and R. S. Fujinami, unpublished data).

Viral antigen was found predominantly in neurons in gray matter lesions in all groups (Fig. 4). Surprisingly, we detected fewer virus-infected cells in both DApB and DApBL2M virus-infected mice (Fig. 5, $P < 0.01$ and $P < 0.05$, respectively), despite the fact that the MNC infiltration was similar between the groups.

Chronic phase neuropathology. During the chronic phase, 1 month after infection, in pDA and DApB virus-infected mice, the gray matter lesions completely resolved. Affected regions were found to be normal in appearance (Fig. 6g) or showed mild gliosis. In the spinal cord, however, we detected MNC infiltration with demyelination in the white matter, especially in the ventral root entry zone (Table 2). To some extent, the anterior and the lateral columns were also involved. Four months after infection, demyelinating disease progressed and large areas were affected in the anterior and lateral columns (Fig. 6a and c). The posterior column, particularly the corticospinal tract and the gracile fasciculus, was relatively spared (47). In the brain, mild MNC infiltration was detected only in the brainstem and demyelination was rare. No difference was seen in the cellular composition and distribution of the lesions between pDA and DApB virus-infected mice. However, pDA virus-infected mice developed more severe lesions than mice infected with DApB virus (Fig. 6a and c). After 4 months, the meningitis score for pDA virus infection was 62.5 ± 7.4, and that of DApB virus infection was 38.8 ± 7.6 ($P < 0.05$); the perivascular cuffing score of pDA virus-infected mice was 35.5 ± 5.3, and that of DApB virus-infected animals was 16.8 ± 4.6 ($P < 0.05$); and the demyelination score of pDA virus infection was 49.3 ± 6.2, and that of DApB virus infected mice was 36.5 ± 8.2.

In contrast, in DApBL2M virus-infected mice, a mild but definite MNC infiltration with pyknotic neurons in the gray matter of the brain, including hippocampus and cerebellum, was present even 4 months after infection (Table 2; Fig. 6h). In the spinal cords 1 month after infection, we detected only mild meningitis; the spinal cords appeared normal 4 months after infection (Fig. 6e).

Viral antigen was found in either glial cells or macrophages (42) in the white matter demyelinating lesions in the spinal cord of pDA and DApB virus-infected mice (Fig. 6b and d). DApB virus-infected mice, however, contained fewer viral antigen-positive cells than pDA virus-infected mice (Fig. 5b). In DApBL2M virus-infected mice, while no viral antigen-positive cells were detected in the spinal cord (Fig. 5 and 6f), viral antigen could be detected in the gray matter of the brain (Fig. 6i). Persistence of DApBL2M virus in the gray matter of the brain was also confirmed by in situ hybridization detecting the viral genome (Fig. 6j). In the hippocampi of DApBL2M virus-infected mice, we detected viral antigen and RNA in cells from five of eight mice 1 month postinfection and in five of six mice 4 months postinfection.

CNS virus titer. To clarify whether there was a correlation between virus replication and pathogenesis, we isolated infectious virus from the brains and spinal cords of mice infected with the TMEVs (Table 3). Although we could see similar clinical and histological disease during the acute phase between pDA, DApB, and DApBL2M virus infections, higher virus titers were detected in pDA virus-infected mice than in mice infected with the mutants. No infectious virus was found in the CNS during the acute phase of DApBL2M virus infection. Thus, virus replication in the brain did not correlate with the neuropathology during the acute phase of TMEV infection. During the chronic phase, we were able to isolate virus from all mice infected with pDA; the highest virus titer was detected in the spinal cord 4 months after pDA virus infection. In contrast, virus was isolated from only a single animal with both DApB and DApBL2M virus infection (Table 3). Altogether, we detected lower amounts of viruses from DApB and DApBL2M virus-infected mice; these results were consistent with the immunohistochemistry data described above. It should be noted that we could not isolate infectious virus by a plaque assay but could detect viral antigen and genome by immunohistochemistry and in situ hybridization during DApBL2M virus infection. This discrepancy could be due to the presence of serum and/or tissue bound anti-TMEV antibody detected during TMEV infection (see below).

Anti-TMEV antibody titer. To exclude the possibility that a difference in the antibody response accounted for differences in virus replication and virus clearance, we compared by ELISA serum anti-TMEV antibody titers between the groups infected with pDA, DApB, and DApBL2M viruses. During the acute phase, 1 week postinfection, we could detect anti-TMEV antibody responses from all groups (Fig. 7); there was no statistical difference between the groups. During the chronic phase, we detected high antibody titers in all groups. However, the titer in the DApBL2M virus-infected group was the lowest. Thus, serum anti-TMEV antibody titer tended to correlate with virus replication or persistence. A less efficient host immune response for CNS virus clearance could not explain virus persistence. The lower amount of anti-TMEV antibody during DApBL2M virus infection could be due to fewer virus-infected cells at late times postinfection, leading to a lack of chronic antigenic stimulation.

DISCUSSION

During the chronic phase, DApB virus-infected mice developed an attenuated demyelinating disease in the white matter of the spinal cord, while DApBL2M virus-infected mice showed prolonged gray matter disease in the brain without lesions in the white matter (Table 4). Therefore, mutations of DA virus in loop structure(s) could alter the virus-cell interaction for persistent infection in the CNS, leading to abortive or no infection of macrophages and glial cells in the white matter of the spinal cord. The virus may use a different receptor on neurons versus macrophages or glial cells. In addition, during the chronic phase of DApBL2M virus infection, we detected lesions exclusively in the brain, not in the spinal cord. There, mutations in DApBL2M might play a key role not only in a shift of the virus from gray to white matter but also in the movement of virus from the brain to the spinal cord.

We previously reported that DA8 mutant virus, which has VP1 loop II of GDVII virus in the background of DA virus, resembled wild-type DA virus with respect to acute and chronic disease and viral replication (Table 4) (49). DApBL2M virus also has VP1 loop II of GDVII virus with a single amino acid mutation in VP2 puff B. Since DApBL2M virus showed less

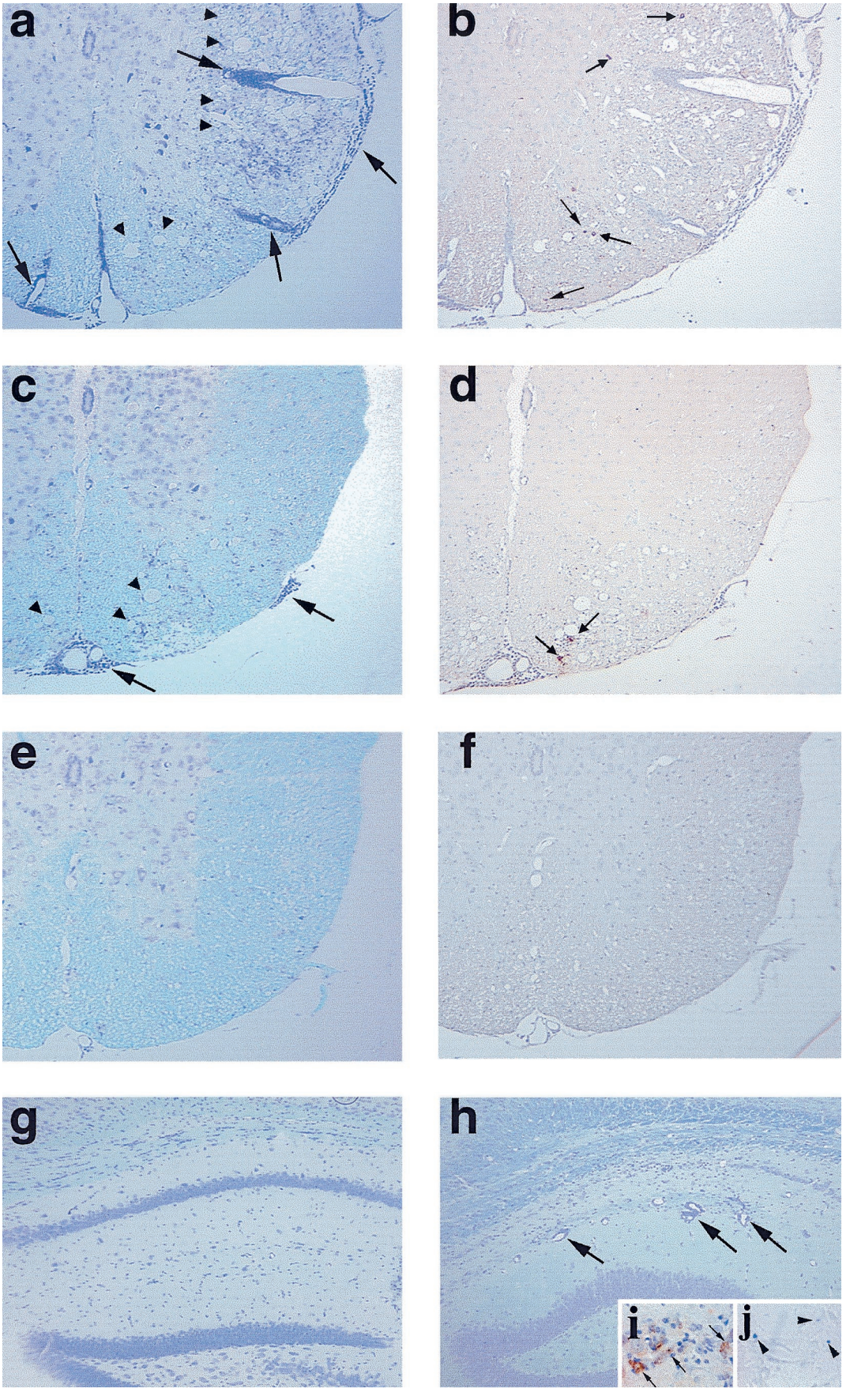
a
b
c
d
e
f
g
h
i
j

TABLE 3. Viral titers in the CNS of the mice infected with pDA, DApB, and DApBL2M

Time postinfection	Titer (PFU/g)[a]					
	pDA		DApB		DApBL2M	
	Brain	Spinal cord	Brain	Spinal cord	Brain	Spinal cord
1 wk	3.3×10^4	2.6×10^4	1.6×10^4	1.7×10^4	—[b]	—
1 mo	2.7×10^3	1.5×10^4	6.6×10^2[c]	—	—	—
4 mo	4.6×10^3	1.6×10^5	—	—	—	7.3×10^2[c,d]

[a] Mean from three mice at each time point.
[b] —, below the detection limit.
[c] Infectious virus was isolated from one of three mice.
[d] Sequence analysis demonstrated that the virus had a single amino acid mutation at position 171 (R to G) that differed from the original DApBL2M virus used to infect the mice.

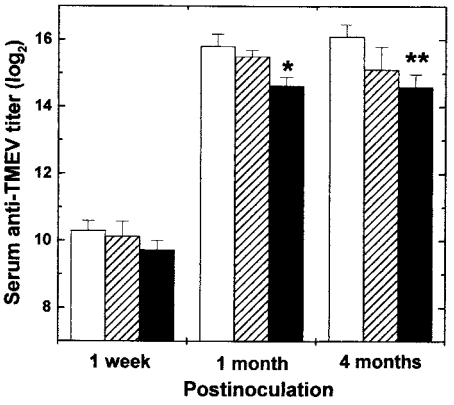

FIG. 7. Serum anti-TMEV antibody titer from the mice infected with pDA (blank columns), DApB (hatched columns), or DApBL2M (closed columns) virus. Using ELISA, we detected serum anti-TMEV antibodies from the mice 1 week and 1 and 4 months after virus infection. Significant anti-virus antibody responses were detected in all groups as early as 1 week postinfection. During the chronic phase, while DApBL2M virus-infected mice produced lower antibody responses (*, $P < 0.05$; **, $P < 0.01$ compared with pDA) than pDA virus-infected mice, we could detect high anti-virus antibody responses in all groups. Each experimental group consisted of six to eight mice.

virus replication than DA8 and a tropism different from that of DA8 (49) in vivo, the additional mutation in VP2 puff B of DApBL2M most likely contributed to the difference in pathology. In contrast, mice infected with another mutant, DApB, had a lesion distribution similar to that of DA virus-infected mice although DApB has three amino acid mutations in VP2 puff B in the background of DA virus. Thus, the conformational alteration composed of two loop structures (DApBL2M) could influence distribution and pathology rather than the single mutation of DA virus either in VP1 loop II (DA8) or in VP2 puff B (DApB). Since VP2 puff B and VP1 loop II are located close to a putative receptor binding site and a gap (51), the conformational changes in the loop structures can influence virus-cell interaction, leading to a difference in tropism and replication in vivo.

Our results support the hypothesis by Adami et al. (1) that persistence depends on a conformational determinant that requires homologous sequences in the VP2 puffs and VP1 loops, which closely interact on the virion surface (10, 23, 24). They made recombinant TMEV in which GDVII virus was progressively replaced starting in the leader with BeAn virus, a strain of the TO subgroup. The recombinant GDVII virus with BeAn virus sequences from the leader to halfway through VP1 (to position 169 of the 276-residue VP1) caused demyelination with virus persistence, while virus with GDVII sequences replaced with BeAn sequences ending upstream of the VP1 loops did not persist. The former contains VP2 puffs and VP1 loops of BeAn virus; the latter encodes VP2 puffs of BeAn and VP1 loops of GDVII virus.

Another TMEV recombinant warranting mention is GD1B-2C/DAFL3, which is partially neurovirulent and persists in the CNS and produces demyelination (6, 32). GD1B-2C/DAFL3 contains GDVII virus sequences in the carboxyl half of VP2 (amino acids 152 to 267) and in VP3 and VP1 on a DA virus background; GD1B-2C/DAFL3 has hybrid VP2 puffs, with puff A containing DA sequences and puff B containing GDVII virus sequences. In these studies, general structural changes due to the recombination in other than loop structures may also affect a putative conformational determinant.

Since DApBL2M replicated less efficiently than pDA virus during the acute phase, this difference in virus replication could hypothetically contribute to the difference in pathology between the two viruses seen during the chronic phase. However, we feel that this is not likely the case. Although a suboptimal dose of TMEV in mice has been reported not to cause demyelinating disease (9), a prolonged gray matter disease as seen in DApBL2M-infected mice has never been reported in studies using suboptimal doses of TMEV to infect mice.

The anti-TMEV antibody against the loop structures might play an important role in infection of microglia and macrophages in the white matter of the spinal cord. In many other virus infections, including dengue virus infection, virus-antibody complexes are known to be taken up more readily than uncoated virus particles by cells expressing Fc receptors, depending on specificity or concentration of antibody. This phe-

FIG. 6. Neuropathology during the chronic phase of TMEV infection. Mice were killed 4 months after pDA (a, b, and g), DApB (c and d), or DApBL2M (e, f and h to j) virus infection. pDA virus-infected mice (a) showed severe inflammation (large arrows) with demyelination in the spinal cord white matter (arrowheads) versus DApB virus-infected mice (c). pDA virus-infected mice (b) have more TMEV antigen-positive cells (small arrows) than DApB virus-infected mice (d). In DApBL2M virus-infected mice, spinal cords appeared normal (e) and no viral antigen-positive cells were detected (f). While no lesions were found in the gray matter of the brain in pDA (g) or DApB virus-infected mice, we could see hippocampus inflammation (h, large arrows) in DApBL2M virus-infected mice similar to that of acute disease, even after 4 months postinfection. During the chronic phase of DApBL2M virus infection, both viral antigen (i, diaminobenzidine stain, brown, arrow) and genome (j, BCIP-NBT, blue, arrowhead) could be detected in the pyramidal cell layer of the hippocampus, using immunohistochemistry and in situ hybridization, respectively. (a, c, e, g, and h) Luxol fast blue stain; (b, d, f, and i) immunohistochemistry for TMEV antigen; (j) in situ hybridization for TMEV genome. Magnifications: a to f, ×70; g to j, ×150.

TABLE 4. Comparison of GDVII, DA, and DA mutants with changes in VP1 loop II and/or VP2 puff B to GDVII

Virus	VP1 loop II	VP2 puff B	Acute phase		Gray matter-white matter shift[a]	Chronic phase	
			Virus replication	MNC infiltration		Virus persistence	Demyelination
GDVII	GD[b]	GD	++++	+	−	−	−
DA	DA[c]	DA	+++	++	+	+++	+++
DApB	DA	GD	++	++	+	+	++
DApBL2M	GD	—[d]	+	++	−	±	−
DA8[e]	GD	DA	+++	++	+	+++	+++

[a] DA, DApB, and DA8 viruses caused gray matter disease during the acute phase and white matter disease during the chronic phase, while GDVII and DApBL2M viruses caused only gray matter disease.
[b] Virus has sequences of GDVII virus either in VP1 loop II or in VP2 puff B.
[c] Virus has sequences of DA virus either in VP1 loop II or in VP2 puff B.
[d] The VP2 puff B of DApBL2M virus has a two-amino-acid reversion of GDVII VP2 puff B.
[e] Results for DA8 virus were published previously (49).

nomenon, termed antibody-dependent enhancement of infection, can lead to more efficient virus infection in Fc receptor-positive cells (11, 35). Similarly, human immunodeficiency virus (HIV) is known to remain infectious with follicular dendritic cells in the presence of neutralizing antibody (3, 12, 37). Follicular dendritic cells can trap antibody-coated HIV on its processes and convert neutralized HIV to an infectious form. VP1 loop II (52) and VP2 puff B (13, 36) are known to have neutralizing B-cell epitopes in DA virus infection. The neutralization of virus by antibody is not necessarily accompanied by permanent or irreversible changes in the viral particle (20, 25). Indeed, Gard (8) demonstrated reactivation of infectivity of TMEV by dilution after neutralization of virus with serum from TO virus-infected mice. Thus, the B-cell epitopes in wild-type pDA virus could enhance virus infection in Fc receptor-positive cells, including macrophages and microglia. In this case, the substitution of B-cell epitopes on VP1 loop II and VP2 puff B in DApBL2M virus might prevent infection of macrophages and microglia in the white matter of the spinal cord.

VP1 loop II and VP2 puff B are known to contain neutralizing B-cell epitopes in DA virus. We substituted both loop structures in the DApBL2M virus. Thus, the mutant could presumably have a modified number of neutralizing epitopes around these sites. This could contribute to an escape of virus from elimination in neurons in the gray matter of the brain. We previously reported that passive administration of neutralizing monoclonal antibody against VP1 loop II leads to clearance of virus from the CNS of nude mice infected with TMEV (7). Thus, humoral immunity is important for protection against elimination of not only extracellular but also intracellular TMEV in the CNS. Antibody-mediated clearance of virus from the CNS has also been reported for rabies virus (5) and alphavirus (19) infections.

Finally, while the two mutants did not replicate as efficiently as the wild-type virus in vivo during the acute phase of TMEV infection, they induced a level of MNC infiltration similar to that of pDA infection. Interestingly, we found more apoptotic neurons in the brains of mice infected with DApB or DApBL2M viruses than those of mice with pDA virus infection (41; Tsunoda and Fujinami, unpublished). Previously, we demonstrated that there were many more apoptotic neurons present in the brains of mice infected with GDVII virus than in those of mice with DA virus infection (45). The extent and number of apoptotic neurons in DApB or DApBL2M virus-infected mice approached that seen during GDVII virus infection. One explanation for this observation is that the VP2 puff B in wild-type DA virus may play a suppressive role in neuronal cell apoptosis. When mice are infected with DApB and DApBL2M viruses that have a mutation in VP2 puff B at position 171, extensive neuronal apoptosis is seen. This possibility is currently being explored. Although direct lytic viral infection in neurons has been believed to be solely responsible for pathogenesis of the acute disease of TMEV infection, host immune and apoptotic responses also seemed to contribute to the pathogenesis of the acute disease. Higher apoptosis of neurons might contribute to the observation of fewer viral antigen-positive cells in mice infected with DApB or DApBL2M virus.

In this report, we demonstrated that a DA virus mutant, DApB, having a puff B similar to that of GDVII virus, showed acute and chronic diseases attenuated but similar to those of wild-type pDA, while DApBL2M, with VP1 loop II of GDVII virus and an additional mutation in VP2 puff B, showed a prolonged gray matter disease without demyelinating disease. We believe that the conformation of the two loop structures, VP2 puff B and VP1 loop II, contributes to the tropism and pathogenesis of TMEV infection.

ACKNOWLEDGMENTS

We thank Diethilde J. Theil and Ingeborg J. McCright for many helpful discussions and Li-Qing Kuang, Kornelia Edes, Marieke Pigmans, Timothy S. Alexander, Jana Blackett, Kristie M. Parker, and Shawn D. Dalton for excellent technical assistance. We are grateful to Kathleen Borick for preparation of the manuscript.

This work was supported by grant NS34497 from NIH.

REFERENCES

1. **Adami, C., A. E. Pritchard, T. Knauf, M. Luo, and H. L. Lipton.** 1998. A determinant for central nervous system persistence localized in the capsid of Theiler's murine encephalomyelitis virus by using recombinant viruses. J. Virol. **72:**1662–1665.
2. **Balashov, K., and H. L. Weiner.** 1999. Multiple sclerosis, p. 195–212. *In* G. S. Eisenbarth (ed.), Medical intelligence unit 13. Endocrine and organ specific autoimmunity. R. G. Landes Company, Austin, Tex.
3. **Burton, G. F., A. Masuda, S. L. Heath, B. A. Smith, J. G. Tew, and A. K. Szakal.** 1997. Follicular dendritic cells (FDC) in retroviral infection: host/pathogen perspectives. Immunol. Rev. **156:**185–197.
4. **Dal Canto, M. C., B. S. Kim, S. D. Miller, and R. W. Melvold.** 1996. Theiler's murine encephalomyelitis virus (TMEV)-induced demyelination: a model for human multiple sclerosis. Methods **10:**453–461.
5. **Dietzschold, B., M. Kao, Y. M. Zheng, Z. Y. Chen, G. Maul, Z. F. Fu, C. E. Rupprecht, and H. Koprowski.** 1992. Delineation of putative mechanisms

involved in antibody-mediated clearance of rabies virus from the central nervous system. Proc. Natl. Acad. Sci. USA **89:**7252–7256.
6. **Fu, J., M. Rodriguez, and R. P. Roos.** 1990. Strains from both Theiler's virus subgroups encode a determinant for demyelination. J. Virol. **64:**6345–6348.
7. **Fujinami, R. S., A. Rosenthal, P. W. Lampert, A. Zurbriggen, and M. Yamada.** 1989. Survival of athymic (*nu*/*nu*) mice after Theiler's murine encephalomyelitis virus twenty-six infection by passive administration of neutralizing monoclonal antibody. J. Virol. **63:**2081–2087.
8. **Gard, S.** 1955. Neutralization of Theiler's virus. Acta Pathol. Microbiol. Scand. **37:**21–30.
9. **Gerety, S. J., M. K. Rundell, M. C. Dal Canto, and S. D. Miller.** 1994. Class II-restricted T cell responses in Theiler's murine encephalomyelitis virus-induced demyelinating disease. VI. Potentiation of demyelination with and characterization of an immunopathologic $CD4^+$ T cell line specific for an immunodominant VP2 epitope. J. Immunol. **152:**919–929.
10. **Grant, R. A., D. J. Filman, R. S. Fujinami, J. P. Icenogle, and J. M. Hogle.** 1992. Three-dimensional structure of Theiler virus. Proc. Natl. Acad. Sci. USA **89:**2061–2065.
11. **Halstead, S. B.** 1994. Antibody-dependent enhancement of infection: a mechanism for indirect virus entry into cells, p. 493–516. *In* E. Wimmer (ed.), Cellular receptors for animal viruses. Cold Spring Harbor Laboratory Press, Cold Spring Harbor, N.Y.
12. **Heath, S. L., J. G. Tew, J. G. Tew, A. K. Szakal, and G. F. Burton.** 1995. Follicular dendritic cells and human immunodeficiency virus infectivity. Nature **377:**740–744.
13. **Inoue, A., Y.-K. Choe, and B. S. Kim.** 1994. Analysis of antibody responses to predominant linear epitopes of Theiler's murine encephalomyelitis virus. J. Virol. **68:**3324–3333.
14. **Jakob, J., and R. P. Roos.** 1996. Molecular determinants of Theiler's murine encephalomyelitis-induced disease. J. Neurovirol. **2:**70–77.
15. **Jarousse, N., R. A. Grant, J. M. Hogle, L. Zhang, A. Senkowski, R. P. Roos, T. Michiels, M. Brahic, and A. McAllister.** 1994. A single amino acid change determines persistence of a chimeric Theiler's virus. J. Virol. **68:**3364–3368.
16. **Jarousse, N., C. Martinat, S. Syan, M. Brahic, and A. McAllister.** 1996. Role of VP2 amino acid 141 in tropism of Theiler's virus within the central nervous system. J. Virol. **70:**8213–8217.
17. **Jnaoui, K., and T. Michiels.** 1998. Adaptation of Theiler's virus to L929 cells: mutations in the putative receptor binding site on the capsid map to neutralization sites and modulate viral persistence. Virology **244:**397–404.
18. **Kurtz, C. I. B., X. Sun, and R. S. Fujinami.** 1995. Protection of SJL/J mice from demyelinating disease mediated by Theiler's murine encephalomyelitis virus. Microb. Pathog. **18:**11–27.
19. **Levine, B., J. M. Hardwick, B. D. Trapp, T. O. Crawford, R. C. Bollinger, and D. E. Griffin.** 1991. Antibody-mediated clearance of alphavirus infection from neurons. Science **254:**856–860.
20. **Li, Q., A. G. Yafal, Y. M. Lee, J. Hogle, and M. Chow.** 1994. Poliovirus neutralization by antibodies to internal epitopes of VP4 and VP1 results from reversible exposure of these sequences at physiological temperature. J. Virol. **68:**3965–3970.
21. **Lin, X., S. Sato, A. K. Patick, L. R. Pease, R. P. Roos, and M. Rodriguez.** 1998. Molecular characterization of a nondemyelinating variant of Daniel's strain of Theiler's virus isolated from a persistently infected glioma cell line. J. Virol. **72:**1262–1269.
22. **Lipton, H. L.** 1980. Persistent Theiler's murine encephalomyelitis virus infection in mice depends on plaque size. J. Gen. Virol. **46:**169–177.
23. **Luo, M., C. He, K. S. Toth, C. X. Zhang, and H. L. Lipton.** 1992. Three-dimensional structure of Theiler murine encephalomyelitis virus (BeAn strain). Proc. Natl. Acad. Sci. USA **89:**2409–2413.
24. **Luo, M., K. S. Toth, L. Zhou, A. Pritchard, and H. L. Lipton.** 1996. The structure of a highly virulent Theiler's murine encephalomyelitis virus (GDVII) and implications for determinants of viral persistence. Virology **220:**246–250.
25. **Mandel, B.** 1961. Reversibility of the reaction between poliovirus and neutralizing antibody of rabbit origin. Virology **14:**316–328.
26. **McCright, I. J., I. Tsunoda, F. G. Whitby, and R. S. Fujinami.** 1999. Theiler's viruses with mutations in loop I of VP1 lead to altered tropism and pathogenesis. J. Virol. **73:**2814–2824.
27. **Michiels, T., N. Jarousse, and M. Brahic.** 1995. Analysis of the leader and capsid coding regions of persistent and neurovirulent strains of Theiler's virus. Virology **214:**550–558.
28. **Oliver, K. R., P. Brennan, and J. K. Fazakerley.** 1997. Specific infection and destruction of dopaminergic neurons in the substantia nigra by Theiler's virus. J. Virol. **71:**6179–6182.
29. **Pevear, D. C., M. Luo, and H. L. Lipton.** 1988. Three-dimensional model of the capsid proteins of two biologically different Theiler virus strains: clustering of amino acid difference identifies possible locations of immunogenic sites on the virion. Proc. Natl. Acad. Sci. USA **85:**4496–4500.
30. **Rauch, H. C., I. N. Montgomery, C. L. Hinman, W. Harb, and J. A. Benjamins.** 1987. Chronic Theiler's virus infection in mice: appearance of myelin basic protein in the cerebrospinal fluid and serum antibody directed against MBP. J. Neuroimmunol. **14:**35–48.
31. **Rodriguez, M., E. Oleszak, and J. Leibowitz.** 1987. Theiler's murine encephalomyelitis: a model of demyelination and persistence of virus. Crit. Rev. Immunol. **7:**325–365.
32. **Rodriguez, M., and R. P. Roos.** 1992. Pathogenesis of early and late disease in mice infected with Theiler's virus, using intratypic recombinant GDVII/DA viruses. J. Virol. **66:**217–225.
33. **Roos, R. P., S. Stein, Y. Ohara, J. Fu, and B. L. Semler.** 1989. Infectious cDNA clones of the DA strain of Theiler's murine encephalomyelitis virus. J. Virol. **63:**5492–5496.
34. **Rossmann, M. G., and A. C. Palmenberg.** 1988. Conservation of the putative receptor attachment site in picornaviruses. Virology **164:**373–382.
35. **Rothman, A. L., and F. A. Ennis.** 1999. Immunopathogenesis of Dengue hemorrhagic fever. Virology **257:**1–6.
36. **Sato, S., L. Zhang, J. Kim, J. Jakob, R. A. Grant, R. Wollmann, and R. P. Roos.** 1996. A neutralization site of DA strain of Theiler's murine encephalomyelitis virus important for disease phenotype. Virology **226:**327–337.
37. **Schrager, L. K., and A. S. Fauci.** 1995. Human immunodeficiency virus. Trapped but still dangerous. Nature **377:**680–681.
38. **Sethi, P., and H. L. Lipton.** 1981. The growth of four human and animal enteroviruses in the central nervous systems of mice. J. Neuropathol. Exp. Neurol. **40:**258–270.
39. **Simas, J. P., and J. K. Fazakerley.** 1996. The course of disease and persistence of virus in the central nervous system varies between individual CBA mice infected with the BeAn strain of Theiler's murine encephalomyelitis virus. J. Gen. Virol. **77:**2701–2711.
40. **Tolley, N. D., I. Tsunoda, and R. S. Fujinami.** 1999. DNA vaccination against Theiler's murine encephalomytlitis virus leads to alterations in demyelinating disease. J. Virol. **73:**993–1000.
41. **Tsunoda, I., and R. S. Fujinami.** 1996. Two models for multiple sclerosis: experimental allergic encephalomyelitis and Theiler's murine encephalomyelitis virus. J. Neuropathol. Exp. Neurol. **55:**673–686.
42. **Tsunoda, I., and R. S. Fujinami.** 1999. Theiler's murine encephalomyelitis virus, p. 517–536. *In* R. Ahmed and I. Chen (ed.), Persistent viral infections. John Wiley & Sons Ltd., Chichester, United Kingdom.
43. **Tsunoda, I., Y. Iwasaki, H. Terunuma, K. Sako, and Y. Ohara.** 1996. A comparative study of acute and chronic diseases induced by two subgroups of Theiler's murine encephalomyelitis virus. Acta Neuropathol. (Berlin) **91:**595–602.
44. **Tsunoda, I., L.-Q. Kuang, N. D. Tolley, J. L. Whitton, and R. S. Fujinami.** 1998. Enhancement of experimental allergic encephalomyelitis (EAE) by DNA immunization with myelin proteolipid protein (PLP) plasmid DNA. J. Neuropathol. Exp. Neurol. **57:**758–767.
45. **Tsunoda, I., C. I. B. Kurtz, and R. S. Fujinami.** 1997. Apoptosis in acute and chronic central nervous system disease induced by Theiler's murine encephalomyelitis virus. Virology **228:**388–393.
46. **Tsunoda, I., I. J. McCright, L.-Q. Kuang, A. Zurbriggen, and R. S. Fujinami.** 1997. Hydrocephalus in mice infected with a Theiler's murine encephalomyelitis virus variant. J. Neuropathol. Exp. Neurol. **56:**1302–1313.
47. **Tsunoda, I., N. D. Tolley, D. J. Theil, J. L. Whitton, H. Kobayashi, and R. S. Fujinami.** 1999. Exacerbation of viral and autoimmune animal models for multiple sclerosis by bacterial DNA. Brain Pathol. **9:**481–493.
48. **Wada, Y., and R. S. Fujinami.** 1993. Viral infection and dissemination through the olfactory pathway and the limbic system by Theiler's virus. Am. J. Pathol. **143:**221–229.
49. **Wada, Y., I. J. McCright, F. G. Whitby, I. Tsunoda, and R. S. Fujinami.** 1998. Replacement of loop II of VP-1 of the DA strain with loop II of the GDVII strain of Theiler's murine encephalomyelitis virus alters neurovirulence, viral persistence and demyelination. J. Virol. **72:**7557–7562.
50. **Wada, Y., M. L. Pierce, and R. S. Fujinami.** 1994. Importance of amino acid 101 within capsid protein VP1 for modulation of Theiler's virus-induced disease. J. Virol. **68:**1219–1223.
51. **Zhou, L., X. Lin, T. J. Green, H. L. Lipton, and M. Luo.** 1997. Role of sialyloligosaccharide binding in Theiler's virus persistence. J. Virol. **71:**9701–9712.
52. **Zurbriggen, A., J. M. Hogle, and R. S. Fujinami.** 1989. Alteration of amino acid 101 within capsid protein VP-1 changes the pathogenicity of Theiler's murine encephalomyelitis virus. J. Exp. Med. **170:**2037–2049.
53. **Zurbriggen, A., C. Thomas, M. Yamada, R. P. Roos, and R. S. Fujinami.** 1991. Direct evidence of a role for amino acid 101 of VP-1 in central nervous system disease in Theiler's murine encephalomyelitis virus infection. J. Virol. **65:**1929–1937.